Haydeeite: A spin-$\frac{1}{2}$ kagome ferromagnet

D. Boldrin,[1] B. Fåk,[2,3] M. Enderle,[2] S. Bieri,[4] J. Ollivier,[2] S. Rols,[2] P. Manuel,[5] and A. S. Wills[1]

[1]*Department of Chemistry, University College London, 20 Gordon Street, London WC1H 0AJ, United Kingdom*
[2]*Institut Laue-Langevin, CS 20156, F-38042 Grenoble Cedex 9, France*
[3]*CEA and Université Grenoble Alpes, INAC-SPSMS, F-38000 Grenoble, France*
[4]*Laboratoire de Physique Théorique de la Matière Condensée, Université Pierre et Marie Curie, CNRS UMR 7600, F-75252 Paris, France*
[5]*ISIS Facility, Rutherford Appleton Laboratory, Chilton, Didcot OX11 0QX, United Kingdom*

The mineral haydeeite, α-MgCu$_3$(OD)$_6$Cl$_2$, is a $S = \frac{1}{2}$ kagome ferromagnet that displays long-range magnetic order below $T_C = 4.2$ K with a strongly reduced moment. Our inelastic neutron scattering data show clear spin-wave excitations that are well described by a Heisenberg Hamiltonian with a ferromagnetic nearest-neighbor exchange $J_1 = -38$ K and an antiferromagnetic exchange $J_d = +11$ K across the hexagons of the kagome lattice. These values place haydeeite in the ferromagnetic part of the phase diagram, close to the cuboc2 type noncoplanar 12-sublattice antiferromagnetic order of cubocahedral symmetry. Diffuse dynamic short-range ferromagnetic correlations observed above T_C persist well into the ferromagnetically ordered phase with a behavior distinct from critical scattering.

Quantum $S = \frac{1}{2}$ spins localized on the two-dimensional kagome lattice of vertex-sharing triangles are highly frustrated magnetic model systems that are predicted to form quantum spin liquids (QSLs) with exotic ground states and excitations [1]. While initial work focused on nearest-neighbor Heisenberg kagome antiferromagnets [2–7], such as the mineral herbertsmithite [8], it has been realized that further neighbor interactions or the antisymmetric Dzyaloshinski-Moriya (DM) interaction, which is intrinsically allowed in the kagome lattice, may lead to even more fascinating ground states [9–12]. Even for the case of classical spins, the kagome lattice with interactions beyond nearest neighbors (NNs) [see Fig. 1(a)] shows a very rich magnetic phase diagram with complex noncoplanar structures such as chiral and multi-**k** magnetic ordering [13–15]. This is illustrated by the uniformly filled areas in Fig. 1(b) for the case of ferromagnetic NN interaction $J_1 < 0$. Very recently, it was shown that for quantum spins, QSL phases "invade" parts of the classical phase diagram [16–18], as shown by the open circles in Fig. 1(b).

An experimental realization of such a system that exemplifies the importance of quantum effects is the mineral kapellasite [19–23], where high-temperature fits to the magnetic susceptibility [22] place it in the area of the phase diagram that corresponds to the noncoplanar 12-sublattice magnetically ordered cuboc2 phase [see the (blue) solid square in Fig. 1(b)]. However, kapellasite does not actually order magnetically, but instead forms a QSL with gapless spinonlike excitations and short-range correlations, which are reminiscent of the cuboc2 phase [21]. Following recent theoretical work [18], it can now be understood that kapellasite falls in the region of the phase diagram where quantum fluctuations favor a chiral gapless spin liquid state labeled CSL-A, which has similar short-range correlations to kapellasite.

In this Rapid Communication, we explore experimentally other parts of the phase diagram shown in Fig. 1(b). By replacing the Zn^{2+} ion [green open circle in Fig. 1(a)] of kapellasite by Mg^{2+}, we expect the J_d exchange integral to change the most. Such a substitution leads to the mineral haydeeite, which orders ferromagnetically [20]. Our inelastic neutron scattering data allow us to characterize the ground state and determine the exchange integrals via spin-wave theory. We find that it is the decrease of $J_d/|J_1|$ that places haydeeite in the ferromagnetic part of the phase diagram rather than in the cuboc2 antiferromagnetic state.

Haydeeite, α-MgCu$_3$(OH)$_6$Cl$_2$, crystallizes in the trigonal $P\bar{3}m1$ space group (No. 164) with lattice parameters $a = 6.2885(1)$ and $c = 5.7271(1)$ Å. It is isostructural with kapellasite [19,20] and also has $S = \frac{1}{2}$ Cu^{2+} spins forming a highly two-dimensional kagome lattice of equilateral corner-sharing triangles. The kagome lattice is sketched in Fig. 1(a) with the main exchange interactions J_1, J_2, and J_d. The diamagnetic Mg^{2+} ions sit at the centers of the hexagons. Note that haydeeite should not be confused with its polymorph "Mg-herbertsmithite" γ-MgCu$_3$(OH)$_6$Cl$_2$, which has the same chemical formula but a different crystallographic structure and different magnetic properties [24].

A 1.75 g powder sample of fully deuterated haydeeite was synthesized using a scaled-up variant of the established method [20,25]. Powder diffraction using x rays and neutrons confirms the crystallographic structure [20] and, as expected, a higher degree of site order than in kapellasite. In haydeeite, there are no Cu ions on the Mg site and about 16% Mg ions reside on the Cu sites, resulting in a slightly diluted kagome lattice.

Measurements of the magnetic susceptibility $\chi(T)$ at a field of $H = 5$ T and the magnetization $M(H)$ at $T = 2$ K show that deuterated and hydrogenated haydeeite have very similar magnetic properties: Ferromagnetic ordering sets in at $T_C = 4.2$ K, the saturated moment is $0.83\mu_B$ per mole of Cu, the Curie-Weiss temperature extracted from a fit of the linear region $150 < T < 300$ K of the inverse susceptibility is $\theta_{CW} = 28 \pm 3$ K, and a drop in χT at low temperatures suggests antiferromagnetic components.

Inelastic neutron scattering measurements on the fully deuterated α-MgCu$_3$(OD)$_6$Cl$_2$ powder sample were performed on the time-of-flight (TOF) spectrometers IN5 and IN4 at the Institut Laue-Langevin, using neutrons with incident energies
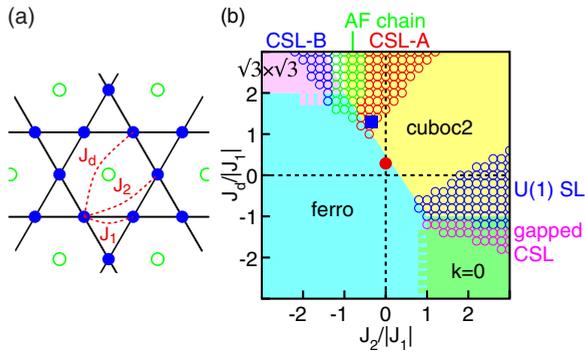
FIG. 1. (Color online) (a) Kagome lattice of haydeeite with Cu^{2+} $S = \frac{1}{2}$ spins (blue solid circles), diamagnetic Mg^{2+} ions (green open circles), and main exchange interactions (red dashed lines). (b) Phase diagram of the kagome lattice for a ferromagnetic nearest-neighbor interaction, $J_1 < 0$. The filled (colored) areas correspond to magnetically ordered phases and the open circles show regions where quantum spin liquid states are predicted [18]. The (blue) solid square represents kapellasite [21,22] while the (red) solid circle corresponds to haydeeite.

E_i of 3.55 and 16.6 meV. These measurements show both acoustic and optic spin-wave branches in the ferromagnetically ordered phase as well as weak magnetic Bragg peaks that are apparent in the difference data (Fig. 2). The high sensitivity, low background, and energy selectivity of the inelastic TOF technique allow us to conclude that these Bragg peaks, which were not observed by standard (energy-integrating) neutron diffraction techniques, probably due to the overlapping strong inelastic diffuse scattering discussed below, correspond to a $k = 0$ propagation vector. Combined with the magnetic susceptibility measurements, this confirms the ferromagnetic ordering.
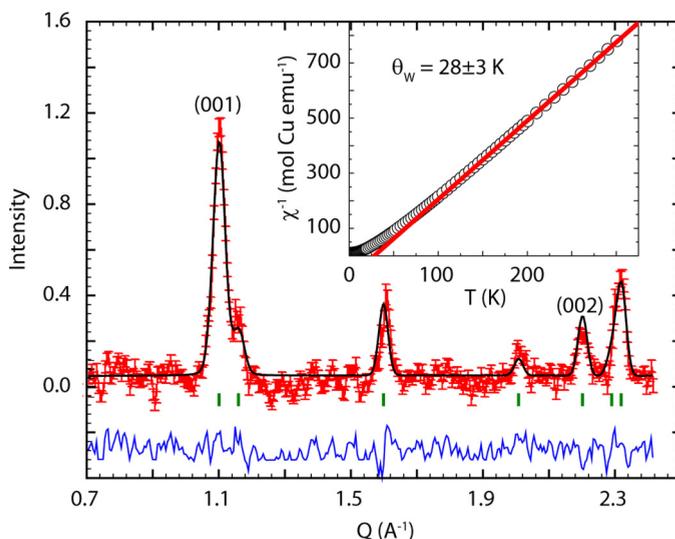

FIG. 2. (Color online) Magnetic Bragg scattering from haydeeite, α-$MgCu_3(OD)_6Cl_2$, obtained by integration over the elastic peak ($|E| < 0.02$ meV) of data from IN5 taken at $T = 1.5$ K after subtraction of 8 K data. The (red) dots are experimental data with 1σ error bars, the solid (black) line going through the data points is the calculated diffraction pattern, and the (blue) line at the bottom is the difference. The inset shows the inverse susceptibility with a linear fit.
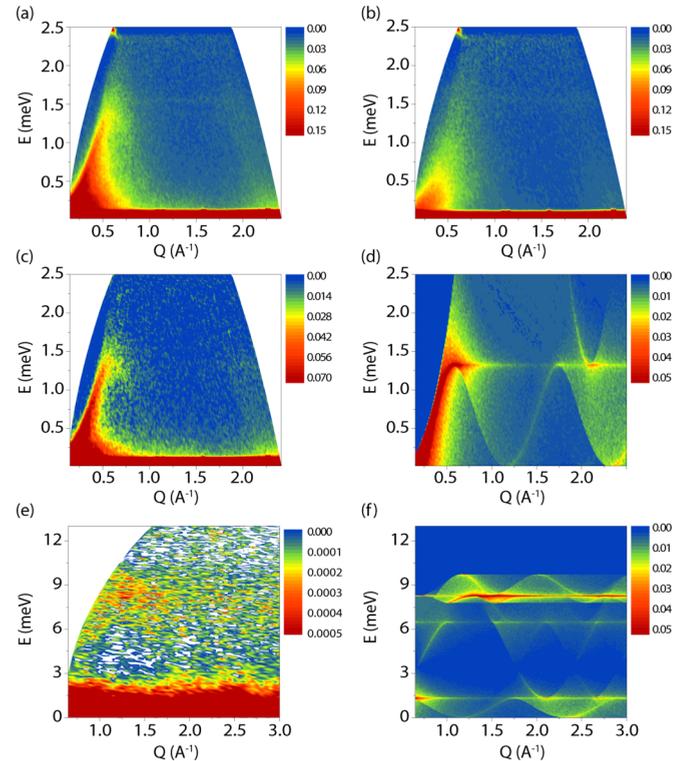

FIG. 3. (Color online) Dynamic susceptibility $\chi''(Q,E)$ on a linear intensity scale as a function of wave vector Q and energy E of fully deuterated haydeeite. Low-energy data measured with $E_i = 3.55$ meV: (a) ferromagnetic state at $T = 1.5$ K, (b) paramagnetic state at $T = 8$ K, and (c) magnetic part of the scattering after subtraction of the $T = 8$ K data. (e) Magnetic scattering at higher energies ($E_i = 16.6$ meV) in the ferromagnetic state at $T = 2.2$ K after subtraction of the high-temperature data at $T = 60$ K. Spin-wave calculations at low and high energies are shown in (d) and (f), respectively.

However, the inelastic TOF technique is not well suited to actually determine the magnetic structure. We have compared on a qualitative level the observed magnetic intensity to that calculated for the three irreducible representations (IRs) [26]. The best description is obtained with a collinear magnetic structure where the moments are in the kagome planes, which corresponds to the two-dimensional Γ_5 IR in Kovalev's notation [27] (see Fig. 2). A rough estimate of the magnetic moment gives a strongly reduced magnitude of at most $0.2\mu_B$ at $T = 1.5$ K, which suggests strong quantum fluctuations.

The observed inelastic neutron scattering intensity is proportional to the dynamic magnetic susceptibility $\chi''(Q,E)$, shown in Fig. 3 for α-$MgCu_3(OD)_6Cl_2$ before correction for the magnetic form factor. Acoustic spin waves are clearly observed in the low-energy data of the ferromagnetically ordered phase shown in Fig. 3(a), and are even more apparent after subtraction of the paramagnetic high-T data of Fig. 3(b) [see Fig. 3(c)]. Optic spin waves are observed at higher energies [see Fig. 3(e)].

The magnetic scattering can be modeled using standard linear spin-wave theory for an isotropic Heisenberg Hamiltonian with further-neighbor interactions. Since haydeeite has three magnetic ions per primitive magnetic unit cell and a
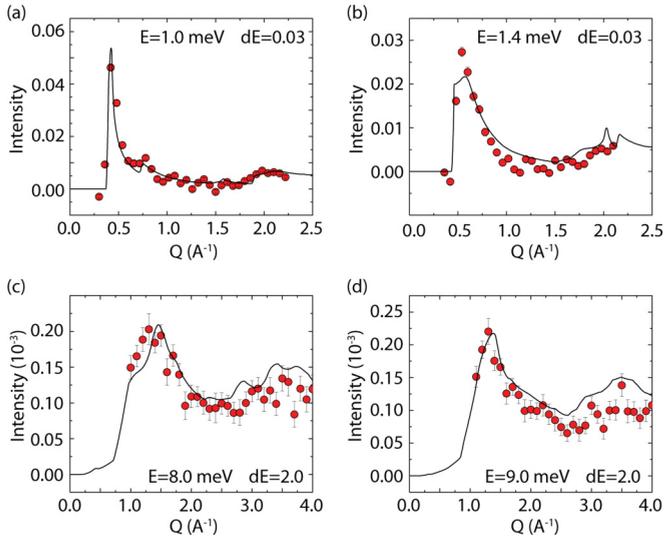
FIG. 4. (Color online) Cuts along Q of the magnetic scattering $\chi''(Q,E)$ at constant energies E as specified in the ferromagnetically ordered phase of haydeeite α-MgCu$_3$(OD)$_6$Cl$_2$ (solid circles) and the powder-averaged spin-wave calculation for $J_1 = -38$ and $J_d = +11$ K (solid line). (a), (b) Excitation energies $E = 1.0 \pm 0.015$ and 1.4 ± 0.015 meV measured with $E_i = 3.55$ meV at $T = 1.5$ K. (c), (d) Excitation energies $E = 8 \pm 1$ and 9 ± 1 meV measured with $E_i = 16.6$ meV at $T = 2.2$ K.
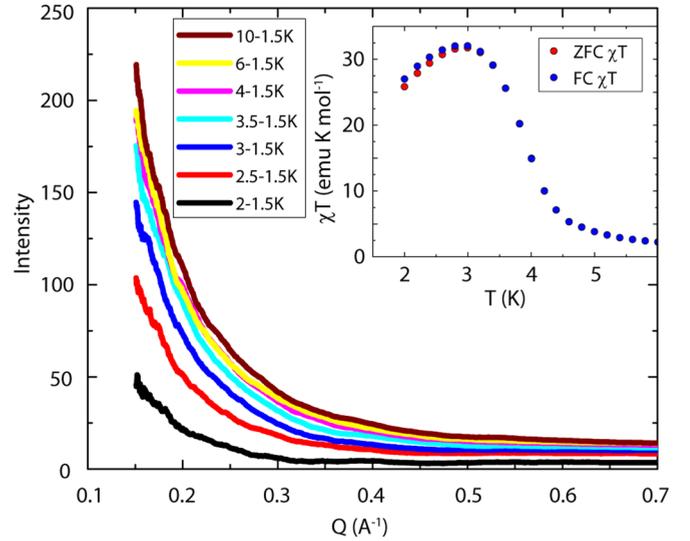

FIG. 5. (Color online) Energy-integrated diffuse scattering from haydeeite for various temperatures after subtraction of the low-T data. Inset: Magnetic susceptibility data χT vs T of α-MgCu$_3$(OD)$_6$Cl$_2$ at $H = 5$ T showing ferromagnetic ordering at $T_C = 4.2$ K and a weak field-cooling/zero-field-cooling (FC-ZFC) splitting at lower temperatures.

propagation vector $k = 0$, there are three spin-wave modes, whose energies and intensities are obtained by diagonalizing a real 3×3 matrix. Standard Monte Carlo techniques are then used to obtain the powder-averaged dynamic susceptibility $\chi''(Q,E)$. The best agreement with the data is found for $J_1 = -38$, $J_2 = 0$, and $J_d = +11$ K, where negative exchange integrals correspond to ferromagnetic interactions and each bond is counted once in the Hamiltonian. The corresponding calculated $\chi''(Q,E)$ is shown in Figs. 3(d) and 3(f). The quality of the agreement is clearly seen in Q cuts at constant energy (see Fig. 4). The calculated spectra are very sensitive to the value of J_2, and from our spin-wave analysis we infer that $|J_2|/|J_1| \ll 0.1$. The Curie-Weiss temperature calculated from these exchanges is $\theta_{CW} = 32$ K, in close agreement with the 28 K estimated from the inverse susceptibility.

Density functional theory (DFT) has predicted a relatively strong antiferromagnetic nearest-neighbor interaction J_1 in both haydeeite and kapellasite [28], in contrast to the ferromagnetic J_1 observed experimentally. Although the sign of J_1 is very sensitive to the O-D distance in the crystallographic structure, a ferromagnetic J_1 is only achieved in the DFT calculations of haydeeite for an O-D distance 20% shorter than the experimentally determined value of 0.98 Å [20]. The origin of this discrepancy is not known.

Diffuse inelastic magnetic scattering is clearly observed at temperatures above T_C, as shown in Fig. 3(b) at $T = 8$ K. In contrast to the kagome antiferromagnets kapellasite ($S = \frac{1}{2}$) [21] and deuteronium jarosite ($S = \frac{5}{2}$) [29], this scattering is clearly dispersive and mimics the spin-wave dispersion, thus resembling so-called paramagnons. Notably, this diffuse scattering seems to coexist with the spin waves below T_C, which can be inferred from the anomalously large Q width of

the scattering [see Fig. 3(a)]. Complementary measurements using the powder diffractometer WISH at ISIS show that the diffuse scattering is centered around $Q = 0$ and corresponds to short-range ferromagnetic correlations with a correlation length of about 35 Å at $T = 6$ K (see Fig. 5). The intensity of the short-ranged ferromagnetic correlations is roughly constant between $T = 3.5$ and 10 K. On further cooling, this intensity decreases, concomitantly with the reduction in χT (see the inset of Fig. 5). The behavior of the rather strong diffuse dynamic magnetic scattering in haydeeite is thus very different from what is expected for frozen-in magnetic disorder and also from critical scattering, for which the correlation length should diverge at T_C. The presence of strong short-range correlations close to a quantum phase transition where ferromagnetic order disappears is intriguing.

We will now discuss the role of the Dzyaloshinski-Moriya interaction in haydeeite. The DM interaction is of current strong interest in kagome ferromagnets [30–33] and kagome antiferromagnets above the saturation field [34], since an out-of-plane DM vector opens up gaps at finite energies in the spin-wave spectrum. This leads to a topological structure of the magnon bands and a finite Berry curvature in momentum space, resulting in the magnon Hall effect [35,36]. The DM interaction is intrinsic to the kagome lattice, since the midpoint of the nearest-neighbor bond lacks inversion symmetry [see Fig. 1(a)]. In haydeeite, just as in the jarosite mineral family [37], the CuO$_6$ octahedra of the crystal structure are tilted with respect to the kagome planes, which allows the DM interaction to have both in-plane, D_{xy}, and out-of-plane, D_z, components [37]. We consider the ferromagnetic case with the assumption that the magnitude of the DM interaction is smaller than $|J_1|$, and use the experimentally determined exchange integrals (see above). For $D_{xy} = 0$, the magnetic structure is a collinear ferromagnet. A finite value of D_{xy} leads to a $k = 0$

umbrella structure with the magnetization perpendicular to the kagome plane and where the opening angle of the umbrella increases with increasing $|D_{xy}|$. A finite value of D_z creates gaps at finite energies of the spin-wave spectrum between the different branches, provided the spins have a component perpendicular to the kagome plane. However, our neutron data are not compatible with the Γ_3 IR that describes an umbrella-type structure with magnetization perpendicular to the kagome planes. Such an umbrella structure should have very low intensity for the (001) and (002) magnetic Bragg peaks, whereas the data show strong intensity there (see Fig. 2). Also, no finite-energy gaps are observed in the spin-wave spectrum. In other words, there is no experimental evidence that the DM interaction plays a significant role in haydeeite.

We conclude that haydeeite appears to be a rare example of an *isotropic* $S = \frac{1}{2}$ Heisenberg kagome ferromagnet. The ordered moment is strongly reduced to $\leqslant 0.2 \mu_B$ and coexists with diffuse dynamic short-range ferromagnetic correlations below T_C. We speculate that the reduction of the ordered moment is due to quantum fluctuations in the proximity to the quantum phase transition between the Heisenberg kagome ferromagnet and the Heisenberg cuboc2 antiferromagnet.

Within this picture, a small increase in the third-neighbor across-hexagon antiferromagnetic exchange interaction J_d would push haydeeite into the magnetically ordered cuboc2 phase, and a further increase of J_d or a slightly ferromagnetic second-neighbor interaction J_2 would lead to a gapless chiral spin liquid state with spinon Fermi surfaces (CSL-A), which breaks reflection and time-reversal symmetries [18]. Such a state may have been observed in kapellasite [21], where the J_d exchange is mediated by Zn^{2+} rather than Mg^{2+} ions. Studies of these compounds under pressure or with some partial Zn-Mg substitution may allow experimental access to quantum spin-$\frac{1}{2}$ kagome systems at the border of a ferromagnetic instability.

[1] L. Balents, Spin liquids in frustrated magnets, Nature (London) **464**, 199 (2010).

[2] M. B. Hastings, Dirac structure, RVB, and Goldstone modes in the kagomé antiferromagnet, Phys. Rev. B **63**, 014413 (2000).

[3] Y. Ran, M. Hermele, P. A. Lee, and X. G. Wen, Projected-wave-function study of the spin-1/2 Heisenberg model on the kagomé lattice, Phys. Rev. Lett. **98**, 117205 (2007).

[4] M. Hermele, Y. Ran, P. A. Lee, and X. G. Wen, Properties of an algebraic spin liquid on the kagome lattice, Phys. Rev. B **77**, 224413 (2008).

[5] S. Yan, D. A. Huse, and S. R. White, Spin-liquid ground state of the $S = 1/2$ kagome Heisenberg antiferromagnet, Science **332**, 1173 (2011).

[6] Y.-M. Lu, Y. Ran, and P. A. Lee, Z_2 spin liquids in the $S = \frac{1}{2}$ Heisenberg model on the kagome lattice: A projective symmetry-group study of Schwinger fermion mean-field states, Phys. Rev. B **83**, 224413 (2011).

[7] Y. Iqbal, F. Becca, and D. Poilblanc, Projected wave function study of Z_2 spin liquids on the kagome lattice for the spin-1/2 quantum Heisenberg antiferromagnet, Phys. Rev. B **84**, 020407(R) (2011).

[8] T. H. Han, J. S. Helton, S. Chu, D. G. Nocera, J. A. Rodriguez-Rivera, C. Broholm, and Y. S. Lee, Fractionalized excitations in the spin-liquid state of a kagome-lattice antiferromagnet, Nature (London) **492**, 406 (2012).

[9] L. Messio, B. Bernu, and C. Lhuillier, Kagome antiferromagnet: A chiral topological spin liquid?, Phys. Rev. Lett. **108**, 207204 (2012).

[10] H. C. Jiang, Z. H. Wang, and L. Balents, Identifying topological order by entanglement entropy, Nat. Phys. **8**, 902 (2012).

[11] L. Messio, C. Lhuillier, and G. Misguich, Time reversal symmetry breaking chiral spin liquids: Projective symmetry group approach of bosonic mean-field theories, Phys. Rev. B **87**, 125127 (2013).

[12] S.-S. Gong, W. Zhu, and D. N. Sheng, Emergent chiral spin liquid: Fractional quantum Hall effect in a kagome Heisenberg model, Sci. Rep. **4**, 6317 (2014).

[13] J.-C. Domenge, P. Sindzingre, C. Lhuillier, and L. Pierre, Twelve sublattice ordered phase in the J_1-J_2 model on the kagome lattice, Phys. Rev. B **72**, 024433 (2005).

[14] J.-C. Domenge, C. Lhuillier, L. Messio, L. Pierre, and P. Viot, Chirality and Z_2 vortices in a Heisenberg spin model on the kagome lattice, Phys. Rev. B **77**, 172413 (2008).

[15] L. Messio, C. Lhuillier, and G. Misguich, Lattice symmetries and regular magnetic orders in classical frustrated antiferromagnets, Phys. Rev. B **83**, 184401 (2011).

[16] R. Suttner, C. Platt, J. Reuther, and R. Thomale, Renormalization group analysis of competing quantum phases in the J_1-J_2 Heisenberg model on the kagome lattice, Phys. Rev. B **89**, 020408(R) (2014).

[17] S.-S. Gong, W. Zhu, L. Balents, and D. N. Sheng, Global phase diagram of competing ordered and quantum spin-liquid phases on the kagome lattice, Phys. Rev. B **91**, 075112 (2015). Note that the exchange called J_3 in this reference refers to the across-hexagon interaction, labeled J_d in our work.

[18] S. Bieri, L. Messio, B. Bernu, and C. Lhuillier, Gapless chiral spin liquid in a kagome Heisenberg model, arXiv:1411.1622.

[19] R. H. Colman, C. Ritter, and A. S. Wills, Toward perfection: Kapellasite, $Cu_3Zn(OH)_6Cl_2$, a new model $S = 1/2$ kagome antiferromagnet, Chem. Mater. **20**, 6897 (2008).

[20] R. H. Colman, A. Sinclair, and A. S. Wills, Comparison between Haydeeite, α-$Cu_3Mg(OD)_6Cl_2$, and Kapellasite, α-$Cu_3Zn(OD)_6Cl_2$, isostructural $S = 1/2$ kagome magnets, Chem. Mater. **22**, 5774 (2010).

[21] B. Fåk, E. Kermarrec, L. Messio, B. Bernu, C. Lhuillier, F. Bert, P. Mendels, B. Koteswararao, F. Bouquet, J. Ollivier, A. D. Hillier, A. Amato, R. H. Colman, and A. S. Wills, Kapellasite: A kagome quantum spin liquid with competing interactions, Phys. Rev. Lett. **109**, 037208 (2012).

[22] B. Bernu, C. Lhuillier, E. Kermarrec, F. Bert, P. Mendels, R. H. Colman, and A. S. Wills, Exchange energies of kapellasite from high-temperature series analysis of the kagome lattice J_1–J_2–J_d-Heisenberg model, Phys. Rev. B **87**, 155107 (2013).

[23] E. Kermarrec, A. Zorko, F. Bert, R. H. Colman, B. Koteswararao, F. Bouquet, P. Bonville, A. Hillier, A. Amato, J. van Tol, A. Ozarowski, A. S. Wills, and P. Mendels, Spin dynamics and disorder effects in the $S = \frac{1}{2}$ kagome Heisenberg spin-liquid phase of kapellasite, Phys. Rev. B **90**, 205103 (2014).

[24] E. Kermarrec, P. Mendels, F. Bert, R. H. Colman, A. S. Wills, P. Strobel, P. Bonville, A. Hillier, and A. Amato, Spin-liquid ground state in the frustrated kagome antiferromagnet $MgCu_3(OH)_6Cl_2$, Phys. Rev. B **84**, 100401 (2011).

[25] D. Boldrin, Synthesis and study of quantum kagome magnets, Ph.D. thesis, University College London, 2015.

[26] A. S. Wills, A new protocol for the determination of magnetic structures using simulated annealing and representational analysis (SARAh), Physica B **276–278**, 680 (2000).

[27] O. V. Kovalev, *Representations of the Crystallographic Space Groups* (Gordon and Breach, Amsterdam, 1993).

[28] O. Janson, J. Richter, and H. Rosner, Modified kagome physics in the natural spin-1/2 kagome lattice systems: Kapellasite $Cu_3Zn(OH)_6Cl_2$ and haydeeite $Cu_3Mg(OH)_6Cl_2$, Phys. Rev. Lett. **101**, 106403 (2008).

[29] B. Fåk, F. C. Coomer, A. Harrison, D. Visser, and M. E. Zhitomirsky, Spin-liquid behavior in a kagomé antiferromagnet: Deuteronium jarosite, Europhys. Lett. **81**, 17006 (2008).

[30] H. Katsura, N. Nagaosa, and P. A. Lee, Theory of the thermal Hall effect in quantum magnets, Phys. Rev. Lett. **104**, 066403 (2010).

[31] R. Matsumoto and S. Murakami, Theoretical prediction of a rotating magnon wave packet in ferromagnets, Phys. Rev. Lett. **106**, 197202 (2011).

[32] L. Zhang, J. Ren, J.-S. Wang, and B. Li, Topological magnon insulator in insulating ferromagnet, Phys. Rev. B **87**, 144101 (2013).

[33] A. Mook, J. Henk, and I. Mertig, Magnon Hall effect and topology in kagome lattices: A theoretical investigation, Phys. Rev. B **89**, 134409 (2014).

[34] E. G. Mishchenko and O. A. Starykh, Equilibrium currents in chiral systems with nonzero Chern number, Phys. Rev. B **90**, 035114 (2014).

[35] K. Ohgushi, S. Murakami, and N. Nagaosa, Spin anisotropy and quantum Hall effect in the kagomé lattice: Chiral spin state based on a ferromagnet, Phys. Rev. B **62**, R6065(R) (2000).

[36] Y. Onose, T. Ideue, H. Katsura, Y. Shiomi, N. Nagaosa, and Y. Tokura, Observation of the magnon Hall effect, Science **329**, 297 (2010).

[37] M. Elhajal, B. Canals, and C. Lacroix, Symmetry breaking due to Dzyaloshinsky-Moriya interactions in the kagomé lattice, Phys. Rev. B **66**, 014422 (2002).